Supplementary information (SI)

Synergistic electronic structure modulation and lattice fortification in hierarchical potassium titanate nanowires for aqueous manganese-ion batteries

Dan Xiang,[a] Qi Lu,[a] Xinhui Li,[a] Qichao Wang,[a] Yang Zheng,[b] Tengfei Zhou*[a]

a Institutes of Physical Science and Information Technology, Key Laboratory of Structure and Functional Regulation of Hybrid Material (Ministry of Education), Anhui University, Hefei 230601, China.
tengfeiz@ahu.edu.cn

b The State Key Laboratory of Refractories and Metallurgy, Institute of Advanced Materials and Nanotechnology, Wuhan University of Science and Technology, Wuhan 430081, China

Experimental Procedures

Experimental Section

Synthesis of Electrode Materials

To synthesize the $K_2Ti_4O_9$ (KTO)

KTO powder, 0.14 mol of potassium hydroxide (KOH) was first dissolved in 40.0 mL of deionized water. Separately, 4 mM of titanium butoxide (TBT) was dissolved in 40.0 mL of ethylene glycol (EG). The TBT-EG solution was then added dropwise to the KOH aqueous solution under continuous stirring for 1 h. The resulting precursor suspension was transferred into a polyphenylene-lined (PPL) autoclave and subjected to a hydrothermal reaction at 200 ℃ for 14 h. Following the reaction, the precipitate was washed repeatedly with ethanol and deionized water until the supernatant reached a neutral pH. Finally, the product was collected and dried in a vacuum oven at 60 ℃ for 12 h to yield pure KTO powder. The B/F co-doped KTO (B/F-KTO) samples were synthesized using an identical protocol, with the exception that stoichiometric amounts of boric acid and potassium fluoride—corresponding to the desired mass ratios—were introduced into the reaction mixture immediately after combining the TBT-EG and KOH solutions.

Electrode Fabrication

Cathodes were prepared by mixing the active material (KTO or B/F-KTO), Super P conductive carbon, and polyvinylidene fluoride (PVDF) binder in a weight ratio of 7:2:1 using N-methyl-2-pyrrolidone (NMP) as the solvent. The resulting slurry was cast onto a stainless steel mesh current collector and vacuum-dried at 80 ℃ for 12 h, yielding a mass loading of approximately 1.0 mg cm^{-2}. Anodes were fabricated by mixing commercial activated carbon (AC), Super P, and PVDF in a weight ratio of 8:1:1 in NMP. This slurry was coated onto carbon felt substrates and vacuum-dried at 80 ℃ for 12 h, resulting in an areal mass loading of approximately 20 mg cm^{-2}.

Electrochemical Measurements

Electrochemical performance was evaluated using CR2032 coin cells assembled in an argon-filled

environment. The full cells utilized the prepared KTO-based cathodes and AC anodes, separated by a glass fiber membrane (Whatman) saturated with 1 M $Mn(CF_3SO_3)_2$ electrolyte. All tests were conducted at approximately 25 ℃within a thermal chamber. Cyclic voltammetry (CV) and electrochemical impedance spectroscopy (EIS) were performed using an Easthua electrochemical workstation. CV profiles were acquired at scan rates ranging from 0.5 to 2.5 mV s^{-1}, while EIS spectra were recorded over a frequency range of 100 kHz to 0.1 Hz. Galvanostatic charge-discharge (GCD), cycling stability, and rate capability tests were carried out on a battery testing system (CT-4008Tn-5V20 mA-HWX) within a voltage window of −1.3 to 0.8 V.

Material Characterization

The morphology and microstructure of the as-prepared samples were examined using field-emission scanning electron microscopy (FESEM, Regulus 8230) and transmission electron microscopy (TEM, JEM-2100). Crystallographic structure was analyzed via X-ray diffraction (XRD, D2 PHASER) utilizing Cu K α radiation at a scan rate of 2 ° min^{-1}. Elemental distribution and composition were verified using energy-dispersive X-ray spectroscopy (EDS) and elemental mapping. Surface chemical states and valence compositions were probed by X-ray photoelectron spectroscopy (XPS, ESCALAB 250Xi), with all binding energies calibrated to the adventitious C 1s peak at 284.8 eV.

The relationship between the peak current (i) and scan rate (v) is governed by the power-law relationship:

$$i = av^b$$

The exponent b identifies the charge storage mechanism: a b -value of 0.5 indicates a diffusion-controlled process, while a value of 1.0 represents a surface-controlled (pseudocapacitive) mechanism.

To further quantify this, the capacitive contribution was partitioned from the total current (i) using the following equation:

$$i = k_1v + k_2v^{1/2}$$

where k_1v and $k_2v^{1/2}$ represent the surface-controlled and diffusion-limited contributions,

respectively.

To elucidate the reaction kinetics during the charge/discharge processes, CV was performed on the *AC*||7*F−KTO* cell at scan rates ranging from 0.5 to 2.5 mV s^{-1}. As illustrated in Figure S11, the CV profiles of the 7*F−KTO* cathode retain congruent shapes and redox features as the scan rate increases, signifying robust electrochemical stability and reversibility. Linear fitting of the redox peaks in Figure 3d yielded -values of 0.73 and 0.53, suggesting that charge storage in the 7*F−KTO* cathode proceeds via a synergistic combination of ion diffusion and pseudo-capacitance.

Supporting Figures：

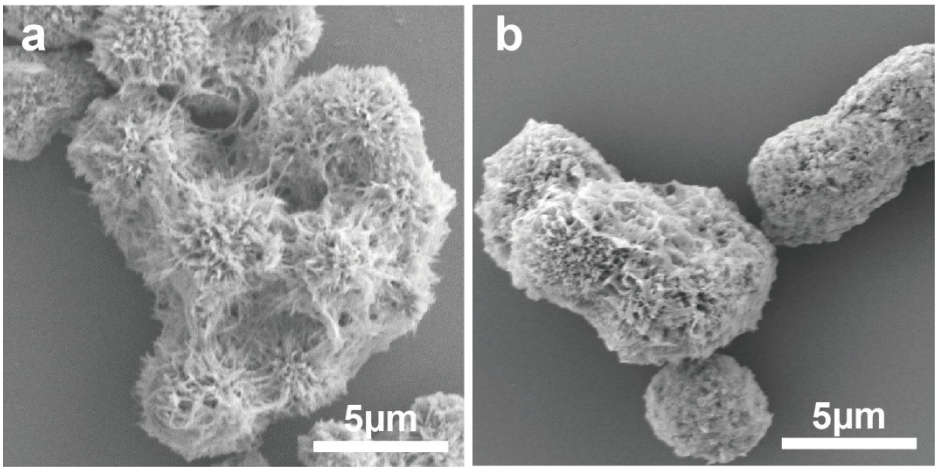

Figure S1. SEM images of (a) 5B-KTO and (b) 7F-KTO.

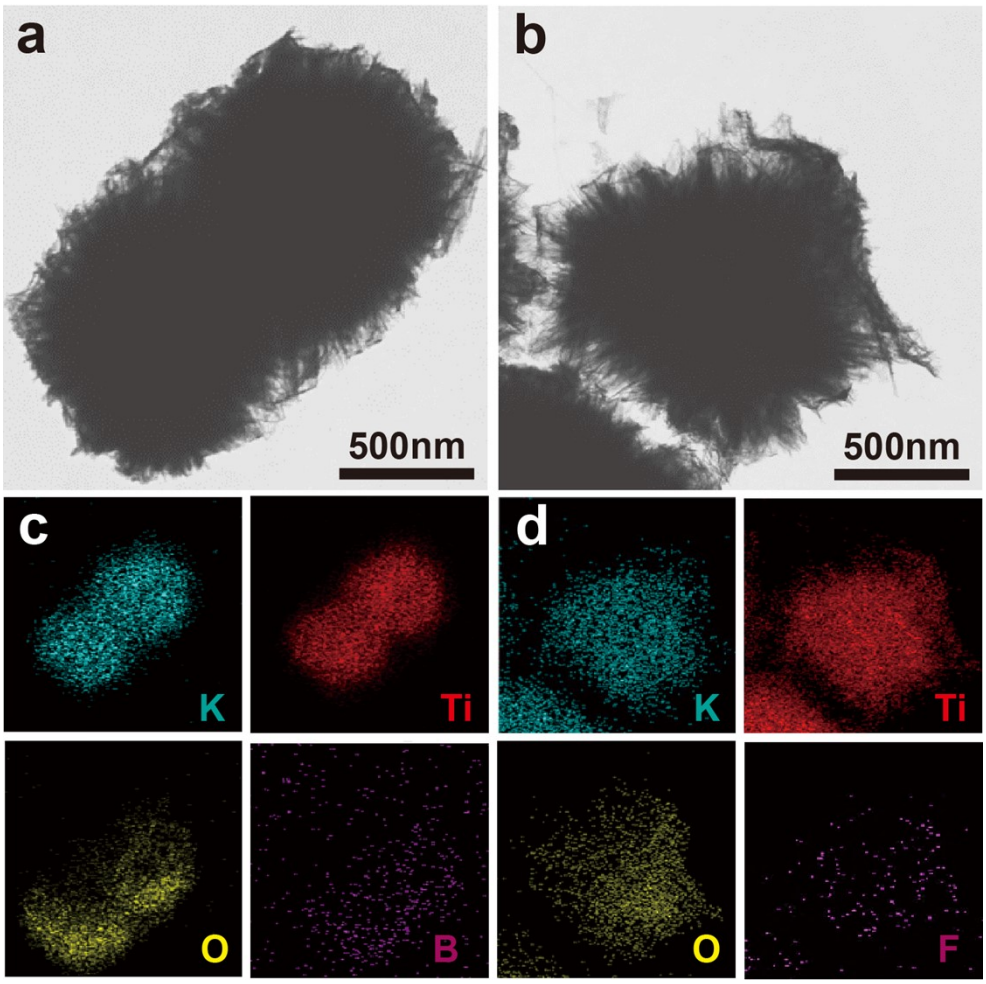

Figure S2. HRTEM images of (a) 5B-KTO and (b) 7F-KTO, Element mapping of (c) 5B-KTO and (d) 7F-KTO.

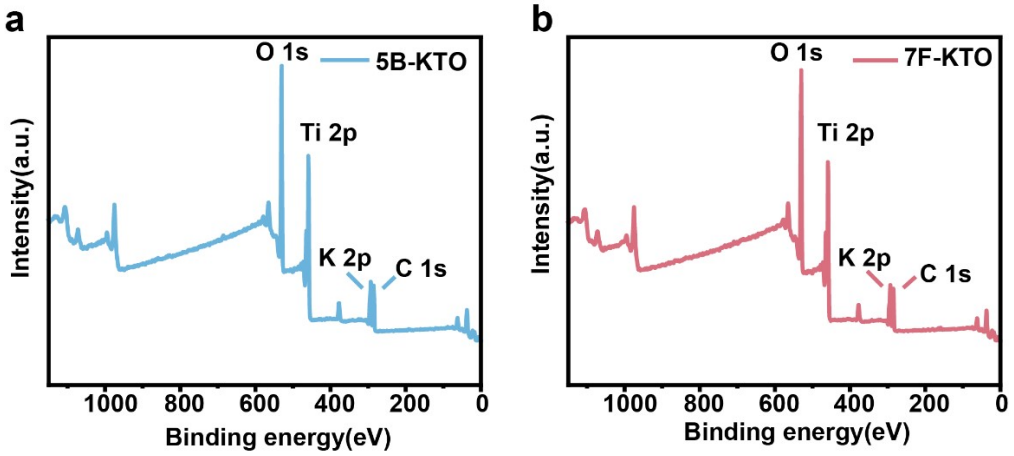

Figure S3. XPS survey scans spectra of (a) 5B-KTO and (b) 7F-KTO.

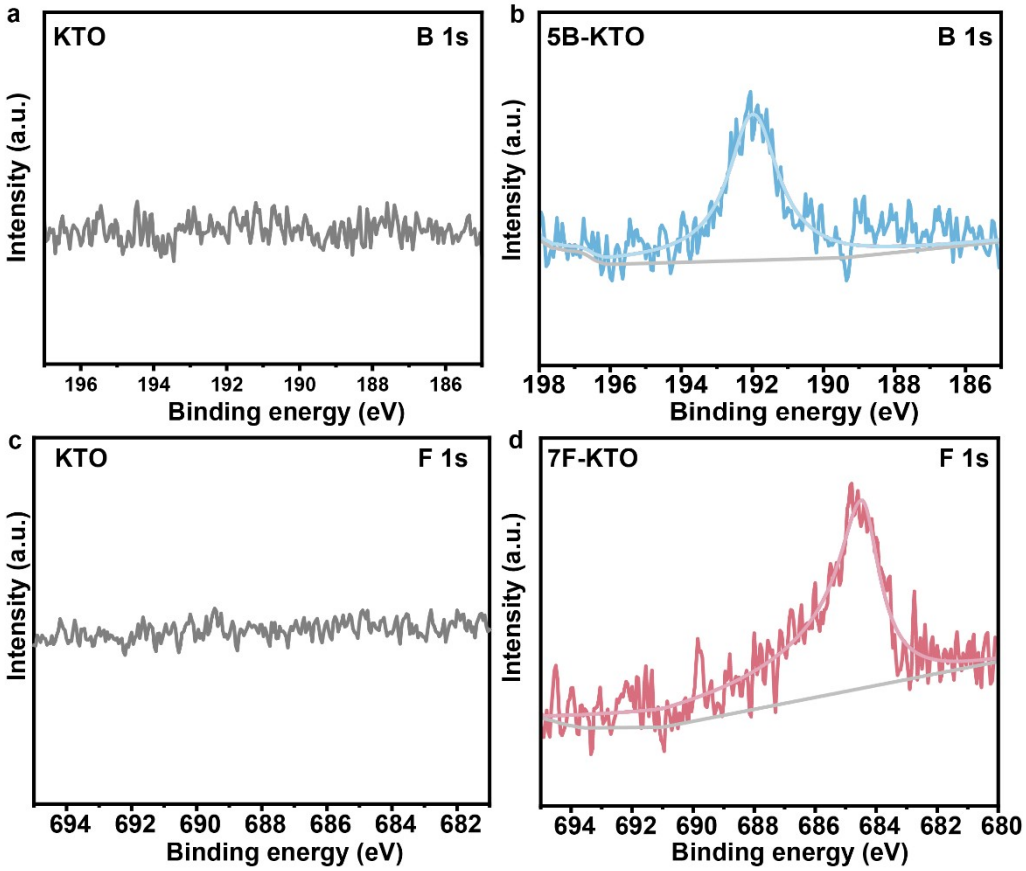

Figure S4. B 1s XPS spectra of (a) KTO and (b) 5B-KTO. F 1s XPS spectra of (c) KTO and (d) 7F-KTO.

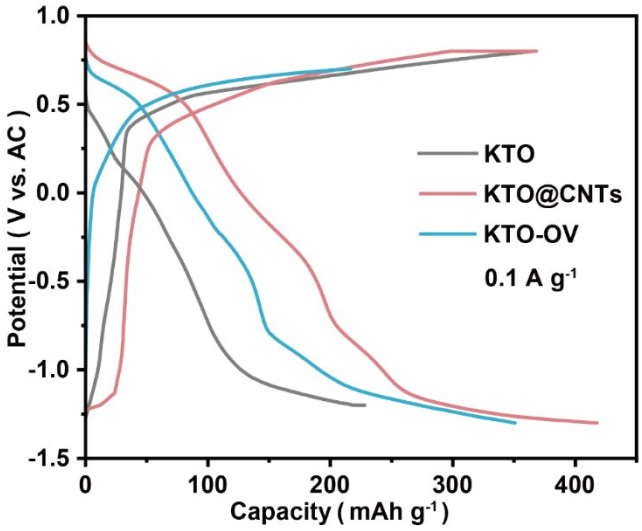

Figure S5. GCD curves of pure KTOs, compounds with carbon nanotubes, and KTO for the creation of oxygen vacancies.

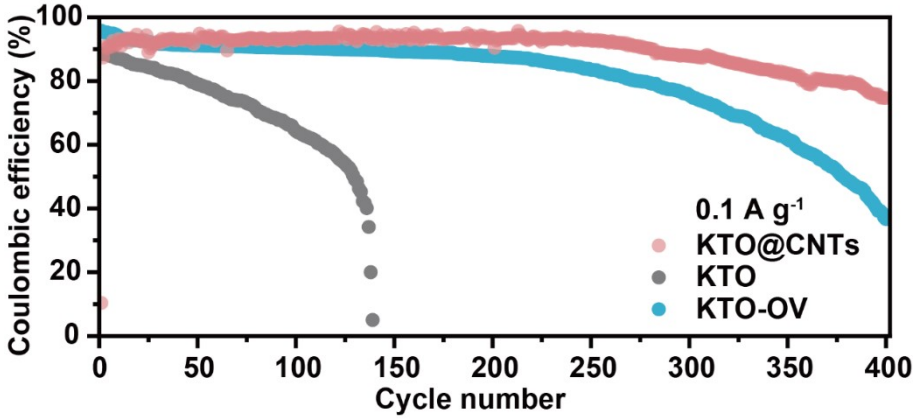

Figure S6. Cycling performance of KTO, KTO@CNTs, KTO-OV cathodes at 0.1 A g^{-1}.

At 0.1 A g^{-1}, KTO@CNTs exhibited an enhanced reversible capacity of 417.7 mAh g^{-1}, compared to 350.8 mAh g^{-1} for the pristine KTO. Conversely, KTO-OV showed a diminished capacity of 227.9 mAh g^{-1}, likely due to lattice instability and accelerated surface side reactions, despite theoretical gains in electronic conductivity. Regarding cyclability, while pristine KTO experienced rapid decay within 150 cycles and KTO-OV retained only 35% after 400 cycles, the KTO@CNTs composite maintained CE of 70%.

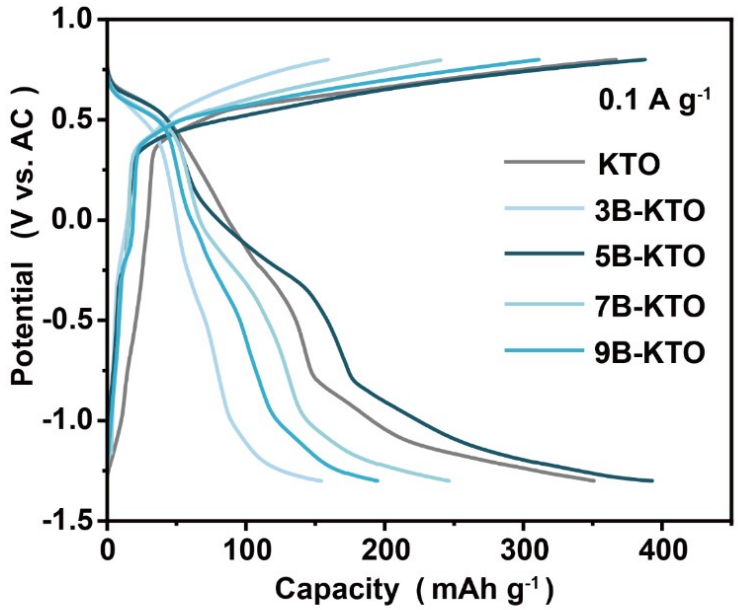

Figure S7. GCD curves of KTO doped with different proportions of B at 0.1 A g^{-1}.

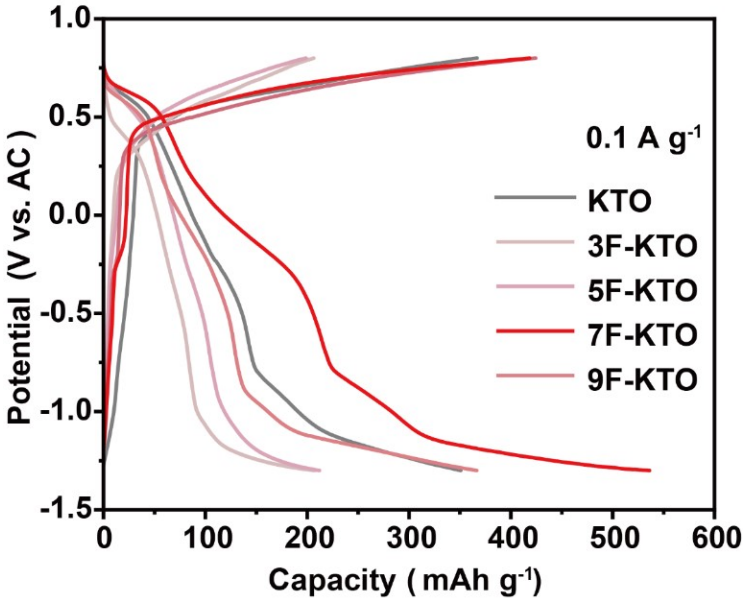

Figure S8. GCD curves of KTO doped with different proportions of F at 0.1 A g^{-1}

A systematic screening of B/F mass ratios was performed to identify the optimal dopant stoichiometry. As shown in Figure S7, the 5B-KTO sample outperformed other boron-doped variants, indicating that moderate boron incorporation facilitates charge storage. In parallel, Figure S8 illustrates the concentration-dependent performance of fluorine-doped. Here, 7F-KTO yielded the highest reversible capacity. Comparing the top performers from both series, 7F-KTO was identified as the optimal composition due to its superior capacity and overall electrochemical kinetics.

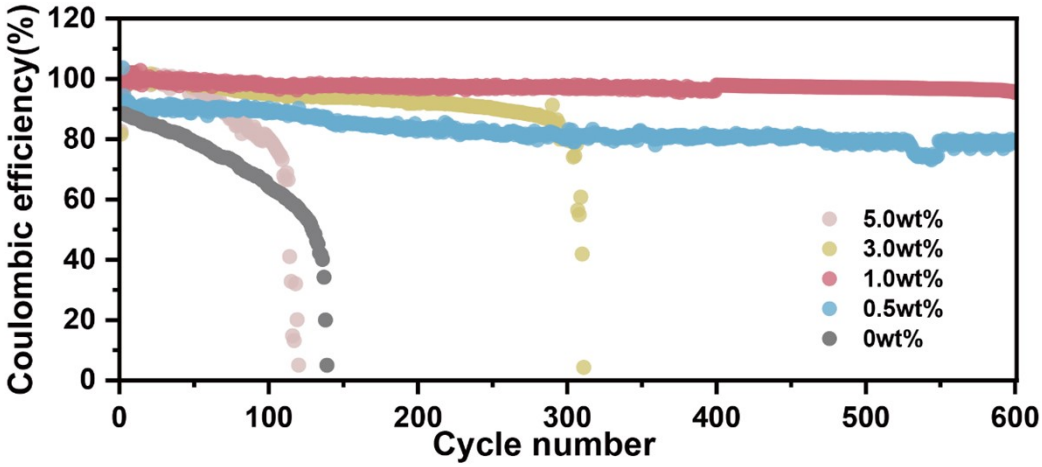

Figure S9. Electrochemical properties of sucrose additives in different proportions of electrolyte.

Subsequent optimization of the electrolyte (Figure S9) involved screening various sucrose concentrations to mitigate parasitic hydrogen evolution. The 1 wt% sucrose additive provided the most significant enhancement in CE and long-term stability. This formulation effectively suppressed side reactions, enabling the full cell to maintain a high CE of 96.5% over 600 cycles at a current density of 2.0 A g^{-1} This confirms that 1 wt% sucrose represents the optimal balance between suppressing side reactions and maintaining electrolyte mobility.

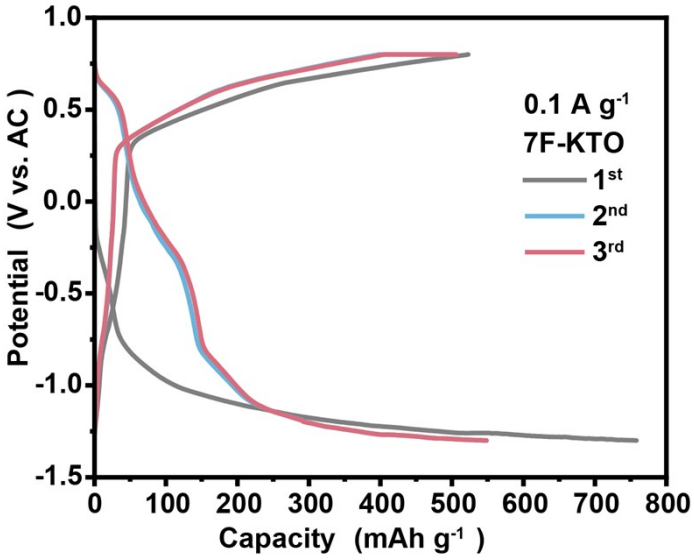

Figure S10. GCD curves of 7F-KTO at the current density of 0.1A g^{-1}.

Figure S11. GCD curves of (a) KTO and (b) 5B-KTO cathode at different specific currents.

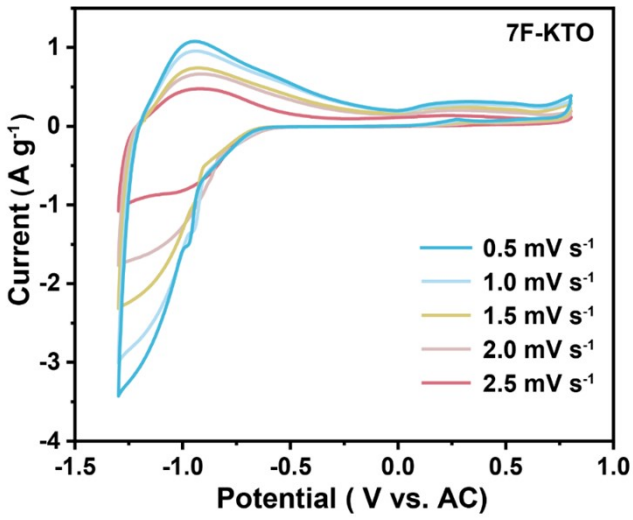

Figure S12. CV curves of 7F-KTO at different scan rate.

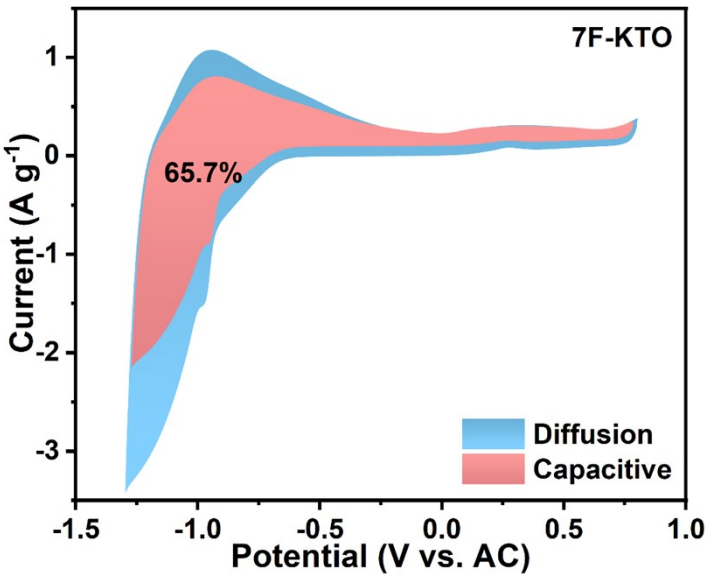

Figure S13. CV curves of 7F-KTO at 2.5 mV s^{-1} for capacitance contribution.

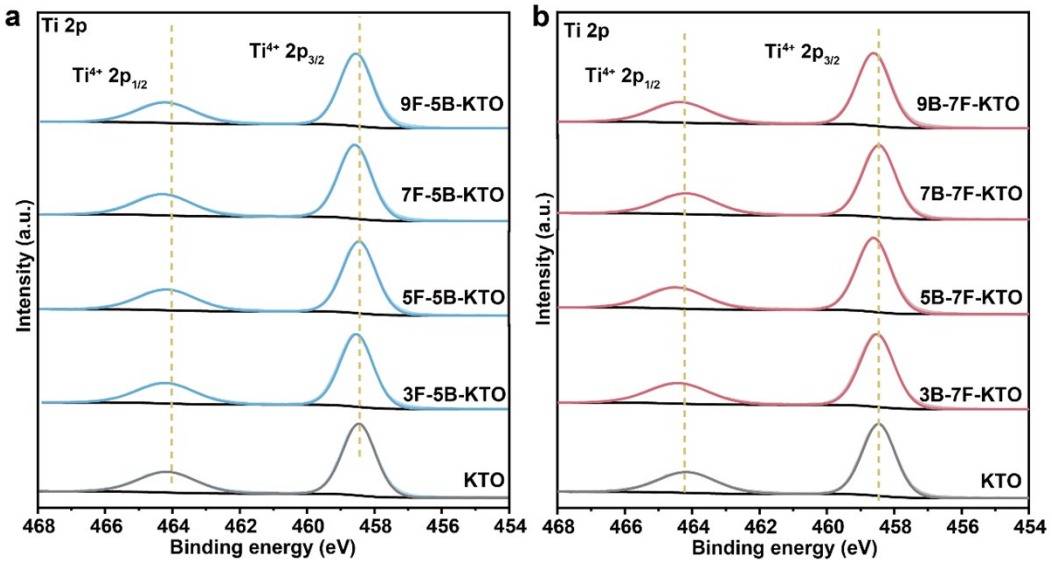

Figure S14. XPS patterns of KTO, (a)doped with F and 5B-KTO and (b)doped with B and 7F-KTO.

Table S1. Comparison of cathode performance between this work and reported works.

Cathode	Specific capacity (mAh g^{-1})	Current density（A g^{-1}）	Cycle number (capacity retention rate)	Ref.
This work: 7F-KTO	**550.3**	**0.1**	**600（98.9%）@2A/g**	-
LiV_3O_8(LVO) nanorods	280	0.1	5000（94%）@3A/g	1
$V_2O_{4.85}$	212.6	0.1	500（89.5%）@0.8A/g	2
VO_2	383	0.5	20000（96.6%）@5A/g	3
Mo_6S_8	93	0.5	1500（96%）@5A/g	4
TCBQ	100	1	500（90.5%）@1A/g	5
PANI	88.3	0.25	1000（67.9%）@0.5A/g	6
$Co(VO_3)_2{\cdot}2H_2O$ (CoVO)	86.1	0.3	1000（65.5%）@0.6A/g	7
$V_2O_{4.85}$	212.6	0.1	500（89.5%）@1A/g	8
Mn-HEPBA	117.9	0.1	5000（82.8%）@1A/g	9
VHCF/HPCF-O	66.5	0.2	10000（102.1%）@10A/g	10
$Cu_{1.8}S$	220	0.02	400（83.3%）@0.5A/g	11
$Al_{0.1}V_2O_5{\cdot}1.5H_2O$ (AlVO)	320.9	0.5	200（85.8%）@1A/g	12
$Mn_{0.18}V_2O_5{\cdot}nH_2O$ (MnVO)	133.7	0.2	200（86.7%）@5A/g	13
$Ag_{0.33}V_2O_5$	261.9	0.1	-	14
$NaV_2(PO_4)_3$ (NVP)	97.2	0.1	2000（85.5%）@0.8A/g	15

Ref:

1. V. Soundharrajan, S. Nithiananth, J. Lee, K. Sakthiabirami, D. Pham, J. Kim,J. Hwang and J. Kim, *J. Power Sources*, 2023, **558**, 232542.
2. S. Lee, H. Lee, H. Lee, S. Baek, N. Shpigel, D. Sharon, S. Hong and M. Chae, *Energy Environ. Mater.*, 2025, **8** ,70036.
3. M. Li, C. Li, C. Zuo, J. Hu, C. Li, W. Luo, S. Luo, A. Duan, J. Wang, X. Wang, W. Sun and L. Mai, *Adv. Mater.*, 2024, **36**, 2407233.
4. A. Nimkar, M. Chae, S. Wee, G. Bergman, B. Gavriel, M. Turgeman, F. Malchik, M. D. Levi, D. Sharon, M. Lukatskaya, N. Shpigel, D. Mandler, *ACS Energy Lett.*, 2022, **7**, 4161 4167.
5. L. Cai, Y. Zhang, W. Yuan, J. Cao, Q. Chen, Y. Lan, F. Zhang, Y. Zhao, J. Shang, and W. Wan, *Adv. Energy Mater.*, 2025, **15**, 2501026.
6. H. Lee, J. Pyun, H. Kwon and M. Chae, *Small*, 2026, **0**, e14020.
7. S. Lee, H. Kwon, S. Baek, J. Pyun, and M. Chae, *Small*, 2026, **22**, e11733.
8. S. Lee, H. Lee, H. Lee, S. Baek, N. Shpigel, D. Sharon, S. Hong and M. Chae, *Energy Environ. Mater.*, 2025, 8, e70036.
9. Z. Xu, Z. Cao, Y. Yang, H. Ren, J. Zhang, J. Yang, L. Long, H. Shao and S. Dong, *Energy Storage Materials*, 2025, **81**, 104457.
10. K. Mao, J. Shao, Y. Huang, W. Tu, J. Li, S. Yang, F. Wang, Y. Gao, P. Zhang and X. Lu, *Adv. Funct. Mater.*, 2025, **0**, e17468.
11. D. Shen, G. Zhao, T. Jiang, H. Liu, R. Luo, Z. Zhang, Z. Zhang, J. Chen, J. Xu, Y. Feng, P. Tong,

S. Tan, Y. Wang, Z. Lv, X. Li and W. Chen, *Angew. Chem. Int. Ed*., 2025, **64**, e202423921.
12. S. Bi, Y. Zhang, S. Deng, Z. Tie and Z. Niu. *Angew. Chem. Int. Ed*., 2022, **61**, e202200809.
13. S. Bi, S. Wang, F. Yue, Z. Tie and Z. Niu, *Nat. Commun.*, 2021, **12**, 6991.
14. H. Lee, A. Nimkar, H. Lee, N. Shpigel, D. Sharon, S. Hong and M. Chae, *Energy Environ. Mater.*, 2024, **8**, e12823.
15. H. Kwon, S. Lee, H. Lee, A. Nimkar, J. Pyun, S. Hong and M.Chae, *Energy Storage Materials*, 2025, **80**, 104406.